

# Design of Microfabricated Inductors for Microprocessor Power Delivery

G. J. Mehas  
K. D. Coonley  
C. R. Sullivan

Found in *IEEE Applied Power Electronics Conference*, Mar. 1999,  
pp. 1181–1187.

©1999 IEEE. Personal use of this material is permitted. However, permission to reprint or republish this material for advertising or promotional purposes or for creating new collective works for resale or redistribution to servers or lists, or to reuse any copyrighted component of this work in other works must be obtained from the IEEE.

Gustavo J. Mehas, Kip D. Coonley, Charles R. Sullivan  
 Thayer School of Engineering  
 8000 Cummings Hall  
 Dartmouth College  
 Hanover, NH 03755-8000  
 gmehas@dartmouth.edu kcoonley@dartmouth.edu chrs@dartmouth.edu  
 603-646-2851 http://engineering.dartmouth.edu/inductor/

*Abstract*—Microfabricated inductor designs are proposed for converters for microprocessor power delivery. The fabrication process uses anisotropic silicon etching to form V-grooves; granular metal/insulator nanoscale composite magnetic materials; and copper conductors. An application specific calculation procedure results in an inductor design with predicted power density over 200 W/cm<sup>2</sup> at 95% efficiency for an 8 MHz, 3.6 V to 1.1 V converter.

## I. INTRODUCTION

The high current requirements (up to 100 A or more) of future microprocessors pose a new challenge for power electronics design. This current must be supplied efficiently at voltages between 1 and 1.5 V, and the voltage must remain stable despite rapid changes in load current. Circuit and control innovations [1], [2], [3], [4], [5], [6], [7], [8] have been developed to improve performance in this application. As discussed in Section II, the inductor is associated with fundamental performance constraints in a buck-converter for this application, and thus is crucial to high-performance power delivery.

Microfabricated thin-film inductors have the potential to provide the characteristics necessary for high performance in microprocessor power delivery. Prototype microfabricated thin-film magnetic components for power conversion have been reported in [9], [10], [11], [12], [13], [14], [15], [16], [17], [18], [19], [20], [21], [22], [23], [24]. However, these designs are limited by low efficiency (often 60% or lower), low power density (often under 1 W/cm<sup>2</sup> of substrate area), or both. In this paper, we propose microfabricated inductor designs incorporating three features that together allow substantial performance improvements for microprocessor power delivery. The proposed designs use new granular composite magnetic materials that reduce losses, are fabricated in V-groove trenches in a silicon substrate to improve efficiency and power density, and are designed specifically to optimize performance for microprocessor power delivery.

## II. INDUCTOR LIMITATIONS FOR MICROPROCESSOR POWER DELIVERY

Consider a typical buck converter supplying a load with a large current step (Fig. 1). If we assume that advanced packaging and interconnect designs have minimized stray inductance such that one lumped capacitor represents bypass capacitance and converter output capacitance, and assume that advanced control operates the power switches in the ideal manner to optimize transient behavior, the smallest possible dip in output voltage due to a load-current step of  $\Delta I$  may be calculated as

$$\Delta V = \frac{(\Delta I)^2 L}{2C(V_{in} - V_{out})} \quad (1)$$

where  $\Delta I$  is the size of the current step,  $L$  is the inductor value,  $C$  is the total bypass and output capacitance, and  $V_{in}$  and  $V_{out}$  are the input and output voltages respectively. This shows that minimizing the inductor value is a key strategy for improving performance; however, reducing the inductor value leads to increased current ripple and higher losses. Increased frequency can be used to reduce the current ripple. The resulting inductor requirement is for low loss with high ripple current and high frequency.

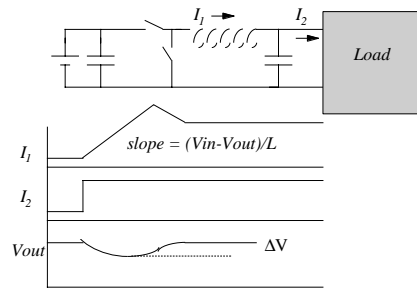


Fig. 1. Constraints on buck-converter response time due to inductor value. Optimized control and negligible stray inductance are assumed.

One attractive choice for ripple current level in the inductor is to allow enough ripple to effect zero voltage switching [1].

### III. MAGNETIC MATERIALS

Microfabricated magnetic components are often made with thin layers of magnetic material to reduce eddy current losses. This is effective at controlling loss resulting from flux traveling in the plane of the film, but flux components out of the plane can still induce eddy currents that result in substantial losses. Unfortunately, the most favorable geometries for transformers and inductors using anisotropic materials such as NiFe include regions with out-of-plane flux [25]. Although multilayer films have been successfully used in thin-film recording heads, power devices typically require a thicker overall layer of magnetic material (e.g.,  $10\ \mu\text{m}$  vs.  $2\ \mu\text{m}$ ), resulting in greater vertical flux travel. In addition, the loss constraints are more stringent in power applications. A transformer geometry using vertically oriented laminations could, in principle, be used to reduce problems with vertical flux travel. However, processing constraints do not allow thin laminations with adequate cross sectional area, and transformers built by this method have low power density and efficiency [26].

An alternative is to use fine particles of metallic magnetic material instead of multilayer thin films, similar in concept to conventional powdered iron materials. Although conventional powdered-metal materials have limited power performance at frequencies this high, recent work has shown that higher performance is possible in vacuum deposited materials with nanoscale particles of Co or Fe [27], [28], [29], [30]. These materials have been fabricated by reactive sputtering. A target such as Co-Al is sputtered in an atmosphere containing a reactive gas such as  $\text{O}_2$ . Ideally, the Al combines with the O and the Co forms a separate phase. Controlling this process to achieve desirable properties in terms of grain size, crystal phase, purity of metal grains, composition of the ceramic matrix, volume fraction of metal, and stress is difficult. Nonetheless, reactive sputtering has demonstrated that such a material can, in fact, have high performance at high frequencies, including relative permeability of 170 and  $Q$  of 60 at 100 MHz, with permeability maintained to about 1 GHz [30], attractive properties for both power and RF applications. In [24], an inductor application of these materials in an efficient high-frequency dc-dc converter was demonstrated at low power density. As described below, improved processes and designs could be combined with these magnetic materials to enable higher performance. In addition, we are currently testing methods of depositing similar materials using vacuum evaporation.

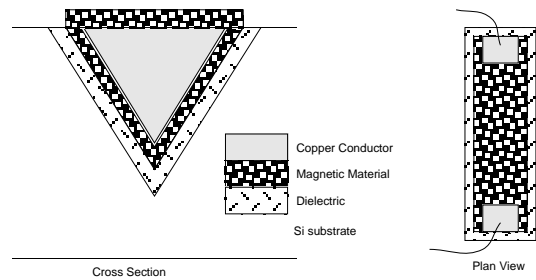


Fig. 2. Schematic diagram of V-groove inductor. Contact pads are indicated on the plan view by “bond wires”, but in practice the interconnection would be accomplished with another metal layer or solder bumps, to avoid high impedance and stray inductance associated with bond wires.

### IV. FABRICATION

A proposed inductor structure is shown in Fig. 2. The one-turn design is preferred for a low-impedance application such as a microprocessor power supply, and allows a simplified process flow. The silicon substrate is anisotropically etched to form V-grooves. Oxide, or other dielectric, is deposited on the silicon. The magnetic material is then deposited on the sloping sidewalls. Ordinarily, deposition of magnetic material on sloping sidewalls is problematic because it is difficult to get favorable properties on both sloped surfaces and flat surfaces [31], [32], [33], [34]. This configuration overcomes these problems: Since this deposition step is used only to deposit on the sloping sidewalls, the process may be set up to optimize magnetic performance, thickness, and other parameters for the sloping surface. Furthermore, grooves bias the orientation of the magnetic anisotropy along their length, which is the desired direction for low hysteresis in an inductor of this design. Following the magnetic material, a metal seed layer is deposited and copper is electroplated to fill the groove. An insulator is not needed between the magnetic material and the copper conductor, because only a single turn is used and the core is insulated from the substrate. The copper may overflow the groove, but is then polished back to planarize the surface before a final deposition of magnetic material. An etch step clears the top of the copper for contacts at the ends. The entire process may be accomplished with only two masks—one for the V-groove definition and one for the final etch.

Fig. 3 shows an inductor design based on a fabrication process such as that in [35], [19]. Comparing this to Fig. 2 illustrates the advantages of the new design. It uses less substrate area, yet it allows more cross sectional area of copper for low dc resistance and allows more surface area of copper for low ac resistance (in fact, the ac resistance is improved even more than this alone would indicate, due to a more favorable field configuration). It reduces the

magnetic path length to minimize core losses and reduces permeability requirements for the magnetic material, and it eliminates the need to simultaneously deposit magnetic material on flat and sloped surfaces.

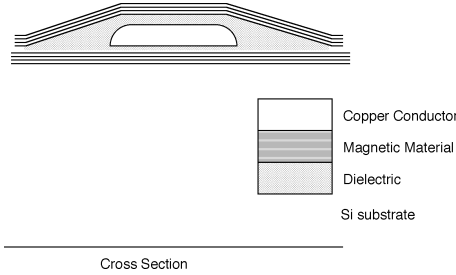


Fig. 3. Schematic diagram of inductor fabricated using a conventional process. The new process improves on these devices by allowing a larger cross sectional area of conductor, decreasing the substrate area required, and decreasing ac losses in both the conductor and magnetic material.

## V. DESIGN CALCULATIONS

Analysis and optimization for microfabricated inductors and transformers is addressed in [36], [25], [19]. Below we develop a similar approach for inductors fabricated with the V-trench process described above and applied to an inductor for a buck converter operating at high frequencies.

Input voltage, output voltage, and output current are insufficient to determine the necessary inductance for a buck converter. One may choose inductance based on ripple current or response time considerations. We choose inductance for a peak-to-peak current ripple of four times the dc output current. This more than suffices to effect the current reversal needed for zero-voltage switching. With this choice of ripple, the inductance required is

$$L = \frac{(1 - D)V_{out}}{4fI_{out}}, \quad (2)$$

where  $D$  is the duty cycle,  $f$  is the frequency, and  $I_{out}$  is the output current.

We now proceed to develop inductor designs based on the V-trench process to meet this inductance requirement. The V-trench design parameters are length, width, core thickness, and core properties (Fig. 4). A reasonable maximum thickness for the core material is  $10 \mu\text{m}$  [19]. The maximum thickness for core material is a preferred choice for most designs of interest, as the high resistivity substantially reduces eddy losses. This leaves three free variables: the width of the inductor, the length of the inductor, and the properties of the magnetic material. In particular, the permeability of the core material is of interest, and one of the advantages of granular

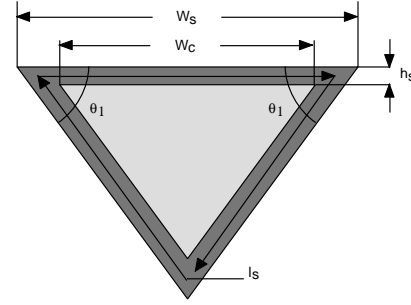


Fig. 4. Geometric parameters used in inductor calculations.  $h_s$  is the thickness of the magnetic material,  $W_s$  is the width of the magnetic material,  $W_c$  is the width of the copper conductor,  $l_s$  is the core flux path length, and  $\theta_1$  is the angle created during an anisotropic etch ( $54.7^\circ$ )

magnetic materials is that their permeability can be varied through changes in material composition [37]. The three parameters (width,  $W_s$ ; length,  $\ell_L$ ; and permeability,  $\mu_r$ ) must be chosen in such a way as to satisfy two constraints: avoiding magnetic saturation and matching the inductance specification (2). This leaves one free parameter that may be varied to effect a desirable tradeoff between the primary performance parameters, which are efficiency and power density.

We choose to use the inductor width ( $W_s$ ) as this free parameter. For a given choice of  $W_s$ , we then select the permeability of the core material and the width of the inductor based on satisfying the constraints of saturation and inductance, respectively (see Appendix A). Each choice of width then results in a complete design, and by calculating the performance of these designs, we can generate a curve of possible performance. An important part of the performance calculation is the prediction of losses, which are calculated as the sum of four quantities: core eddy current losses, core hysteresis, conductor dc losses and conductor ac losses. Our calculation of these quantities, detailed below, assumes the conservative material properties listed in Table I.

Core eddy current losses are a function of the amplitude of the ac flux ( $B_{ac}$ ) which in turn is approximated as

$$B_{ac} = \frac{\sqrt{2}I_{rms}\mu_0\mu_r}{\ell_s}, \quad (3)$$

where  $I_{rms}$  is the rms ac current in the inductor, and  $\sqrt{2}$  converts from rms value to amplitude. With this approximation, the eddy current losses are calculated by

$$P_{core-eddy} = \frac{\omega^2 B_{ac}^2 V_s h_s^2}{24N_s^2 \rho_s}, \quad (4)$$

where  $\omega$  is the frequency in rad/s and  $V_s$  is the volume of the core. Eddy current losses may additionally be reduced by using multiple core layers,  $N_s$ . The materials

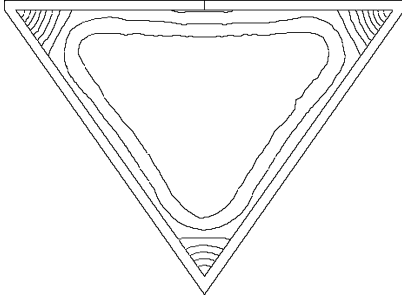


Fig. 5. Contour lines of ac current density calculated by finite element analysis.

described in Section III have sufficiently high resistivity to make the use of multiple layers unnecessary. The core hysteresis loss is modeled as

$$P_{core-hysteresis} = 3B_{ac}fH_cV_s, \quad (5)$$

where  $H_c$  is the coercivity of the core. The factor of three is used to roughly compensate for the non-quadrilateral nature of the hysteresis loop.

Winding losses in the copper of the inductor are modeled as dc and ac power dissipation. Dc power loss is a simple calculation based on the cross sectional area of the copper, the length of the inductor, and the known dc current. Calculating the area of ac current flow in the conductor is more involved, because at high frequencies, skin effect cannot be neglected. We approximated the ac conduction region as roughly a skin depth around the perimeter of the copper. Current crowding at the corners, as seen in Fig. 5, is accounted for as detailed in Appendix B.

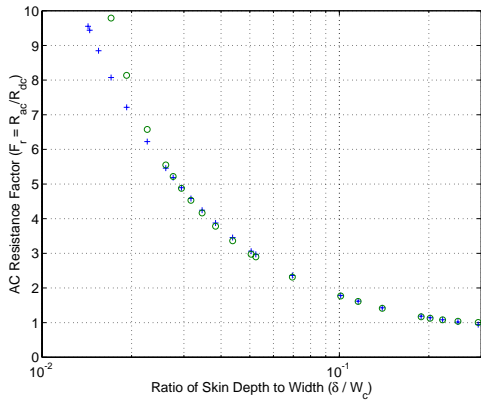


Fig. 6. A comparison between calculated ac resistance (o) in ohms per meter, and the results of the finite element analysis (+). Both resistances are plotted versus skin depth ( $\delta$ ) divided by conductor width ( $W_c$ ).

The ac copper losses were compared with results from the electromagnetic finite element analysis package Maxwell. Fig. 5 shows the simulated current distribution. A correction factor was chosen to make the  $R_{ac}$  calculation match the finite element solution to within 4% over a wide range of width-to-skin depth ratios, as seen in Fig. 6. The total power loss in the inductor is the sum of these four losses.

TABLE I  
INDUCTOR DESIGN FOR 7 A, 1.1 V OUTPUT CONVERTER.

Symbol	Value
$W_c$	Width of conductor 421 $\mu\text{m}$
$h_s$	thickness of magnetic material 10 $\mu\text{m}$
$\ell$	Length 7.16 mm
	Total device width 460 $\mu\text{m}$
$A$	Substrate area 0.033 $\text{cm}^2$
$f$	Operating frequency 8 MHz
$B$	Peak flux density 1 T
$\rho_c$	Conductor (Cu) resistivity 1.8 $\mu\Omega\text{-cm}$
$\rho_s$	Core (Co-Mg-F) resistivity 500 $\mu\Omega\text{-cm}$
$\mu$	Core permeability 45 $\mu_0$
$P$	Converter power output 7.7 W
$P/A$	Power density 233 $\text{W/cm}^2$
$L$	Inductance 3.4 nH
$Q$	Quality factor 20.5
$H_c$	Coercivity 80 A/M
	Core loss 96 mW
$\delta/W_c$	ratio of skin depth to conductor width 0.057
$R_{ac}$	AC resistance 5.72 $\text{m}\Omega$
$R_{dc}$	DC resistance 2.1 $\text{m}\Omega$
	Conductor loss 311 mW
$\eta$	Efficiency 95%

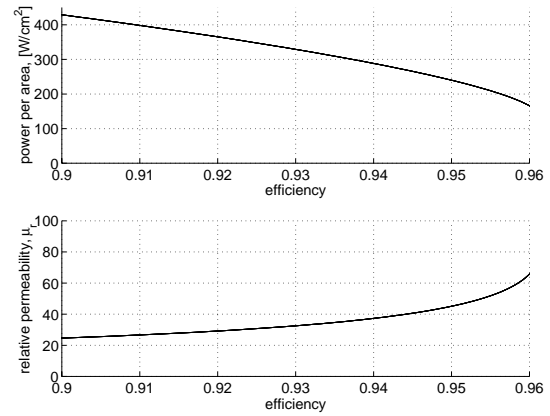


Fig. 7. Design tradeoff in V-groove inductor.

Table I shows a set of specifications, and the results of our calculations based on these specifications. An important design tradeoff, explored in Fig. 7, shows the maximum power density in watts per square centimeter of substrate area as a function of efficiency and the required permeability of the magnetic material for optimum performance, also as a function of efficiency. The permeabil-

ities, in the range of 20 to 100, are similar to the permeabilities found in nanoscale composite magnetic materials.

## VI. AIR-CORE INDUCTORS

Because designs like this call for inductances in the range of a few nH, it might appear that air-core inductors using no magnetic material would be adequate. One problem with many air core designs is unconstrained flux that may induce loss in nearby conductors and cause EMI problems. A shorted coaxial line is one air-core inductor design that avoids this problem. It has the additional advantage that the ac current is distributed uniformly over the conductor surfaces for low ac resistance. With the same circuit requirements, a design optimization was performed for a coaxial cable. Using standard transmission line equations [38] for the inductance per unit length of a coaxial cable with no magnetic material, calculations showed a power density of 32 W/cm<sup>2</sup> at 95% efficiency. Although this is acceptable performance, it is significantly lower than the performance of the V-trench design with granular magnetic materials. This is expected as a low-loss magnetic material can increase the inductance by up to a factor of  $\mu_r$  with little effect on losses, thus increasing  $Q$  by nearly the same factor.

## VII. CONCLUSION

We expect our V-trench process combined with an optimized inductor design to yield substantial performance improvements for microprocessor power delivery with 200 W/cm<sup>2</sup> at 95% efficiency. The V-trench process should require fewer and simpler processing steps in its fabrication. The use of new granular composite magnetic materials aids the reduction of the losses in this new design. These advancements are expected to allow high-frequency, high- $Q$  inductors for microprocessor power delivery applications to become possible.

## APPENDIX

### I. PERMEABILITY AND LENGTH CALCULATIONS

The required relative permeability ( $\mu_r$ ), based on operating at a maximum flux level of 1 T, can be expressed as a function of the core flux path length which is geometrically related to  $W_s$ . The relative permeability is also a function of the maximum allowable flux,  $B_{peak}$ , and the peak current in the inductor,  $I_{peak}$ .

$$\mu_r = \frac{\ell_s B_{peak}}{I_{peak} \mu_0} \quad (6)$$

where  $\mu_0$  is the permeability of free space. One of the benefits of granular magnetic materials is that their permeability can be easily varied through changes in material composition [37].

With width ( $W_s$ ) and relative permeability fixed, the length of the inductor ( $\ell_L$ ) is calculated to meet the inductance requirement (2).

$$\ell_L = \frac{L \ell_s}{\mu_0 \mu_r h_s} \quad (7)$$

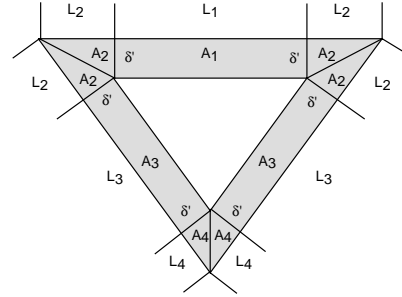


Fig. 8. Lengths and areas used for calculating the ac resistance of the conductor.

### II. $R_{ac}$ CALCULATIONS:

Our  $R_{ac}$  approximation begins by dividing the conductor's perimeter and area as shown in Fig. 8. The parameter  $\delta'$  is the skin depth within the conductor times a constant we selected in order to make our calculation matched the finite element analysis solution. We then assume that current only flows within the shaded regions of the conductor. The approximate amount of current that flows in each area is proportional to the ratio of the length of the corresponding side to the total perimeter of the conductor. After defining the area, current, and the resistivity of the conductor, we can calculate the total ac resistance per meter of the conductor.

More detail on this calculation is available at [http://engineering.dartmouth.edu/inductor/rac\\_calc.html](http://engineering.dartmouth.edu/inductor/rac_calc.html).

### REFERENCES

- [1] A. J. Stratakos, C. R. Sullivan, S. R. Sanders, A. P. Chandrakasan, and R. W. Brodersen, *DC Power Supply Design in Portable Systems*, Kluwer Academic Publishers, 1995.
- [2] A. J. Stratakos, C. R. Sullivan, S. R. Sanders, and R. W. Brodersen, "DC power supply design in portable systems", 1995, Memorandum No. UCB/ERL M95/4.
- [3] S.R. Sanders, Albert Wu, and R. Rossetti, "Active clamp circuits for switchmode regulators supplying microprocessor loads", in *28th Annual IEEE Power Electronics Specialists Conference*, pp. 1179–1185, 1997.
- [4] Xunwei Zhou, Xingzhu Zhang, Jianguang Liu, Pit-Leong Wong, Jibin Chen, Ho-Pu Wu, L. Amoroso and F.C. Lee, and D.Y. Chen, "Investigation of candidate VRM topologies for future microprocessors", in *Thirteenth Annual Applied Power Electronics Conference and Exposition*, pp. 145–50, 1998.
- [5] H.P. Yee, "PWM ASIC suited for power managed  $\mu$  processors", in *Thirteenth Annual Applied Power Electronics Conference and Exposition*, vol. 2, pp. 731–6, 1998.
- [6] G. Schuellein, "Current sharing of redundant synchronous buck regulators powering high performance microprocessors using the

- v<sup>2</sup> control method”, in *Thirteenth Annual Applied Power Electronics Conference and Exposition*, vol. 2, pp. 853–9, 1998.
- [7] R. Redl, B.P. Erisman, and Z. Zansky, “Optimizing the load transient response of the buck converter”, in *Thirteenth Annual Applied Power Electronics Conference and Exposition*, vol. 1, pp. 170–6, 1998.
- [8] Brian Acker, Charles R. Sullivan, and Seth R. Sanders, “Synchronous rectification with adaptive timing control”, in *26th Annual Power Electronics Specialists Conf.*, pp. 88–95, 1995.
- [9] Kiyohito Yamasawa, Kenji Maruyama, Isao Hirohama, and Paul Biringer, “High-frequency operation of a planar-type microtransformer and its application to multilayered switching regulators”, *IEEE Trans. on Magnetics*, vol. 26, pp. 1204–1209, May 1990.
- [10] T. Yachi, M. Mino, A. Tago, and K. Yanagisawa, “A new planar microtransformer for use in micro-switching-converters”, *IEEE Trans. on Magnetics*, vol. 28, pp. 1969–73, 1992.
- [11] T. Yachi, M. Mino, A. Tago, and K. Yanagisawa, “A new planar microtransformer for use in micro-switching-converters”, in *22nd Annual Power Electronics Specialists Conf.*, pp. 1003–1010, June 1991.
- [12] M. Mino, T. Yachi, A. Tago, K. Yanagisawa, and K. Sakakibara, “Microtransformer with monolithically integrated rectifier diodes for micro-switching converters”, in *24th Annual Power Electronics Specialists Conf.*, pp. 503–508, June 1993.
- [13] M. Mino, T. Yachi, K. Yanagisawa, A. Tago, and K. Tsukamoto, “Switching converter using thin film microtransformer with monolithically-integrated rectifier diodes”, in *26th Annual Power Electronics Specialists Conf.*, pp. 665–670, June 1995.
- [14] K. Yamaguchi, E. Sugawara, O. Nakajima, and H. Matsuki, “Load characteristics of a spiral coil type thin film microtransformer”, *IEEE Trans. on Magnetics*, vol. 29, pp. 3207–3209, 1993.
- [15] Kazuyuki Yamaguchi, Shigehiro Ohnuma, Takao Imagawa, Jirou Toriu, Hidetoshi Matsuki, and Koichi Murakami, “Characteristics of a thin film microtransformer with circular spiral coils”, *IEEE Trans. on Magnetics*, vol. 29, pp. 2232–2237, 1993.
- [16] M. Mino, K. Tsukamoto, K. Yanagisawa, A. Tago, and T. Yachi, “A compact buck-converter using a thin-film inductor”, in *Proceedings of Applied Power Electronics Conference, APEC '96*, pp. 422–6, Mar.
- [17] Charles R. Sullivan and Seth R. Sanders, “Measured performance of a high-power-density microfabricated transformer in a dc-dc converter”, in *27th Annual Power Electronics Specialists Conf.*, vol. 1, pp. 287–294, June 1996.
- [18] T. Sato, Y. Miura, S. Matsumura, K. Yamasawa, S. Morita, Y. Sasaki, T. Hatana, and A. Makino, “New applications of nanocrystalline Fe(Co-Fe)-Hf-O magnetic films to micromagnetic devices”, *J. of Applied Physics*, vol. 83, pp. 6658–6660, 1998.
- [19] Luca Daniel, Charles R. Sullivan, and Seth R. Sanders, “Design of microfabricated inductors”, in *27th Annual Power Electronics Specialists Conf.*, vol. 2, pp. 1447–1455, June 1996.
- [20] Chong H. Ahn and Mark G. Allen, “A comparison of two micro-machined inductors (bar- and meander-type) for fully integrated boost DC/DC power converters”, *IEEE Trans. on Power Electronics*, vol. 11, pp. 239–245, Mar. 1996.
- [21] J. Y. Park and M. G. Allen, “Low temperature fabrication and characterization of integrated packaging-compatible, ferrite-core magnetic devices.”, in *IEEE Applied Power Electronics Conf. Proceedings*, vol. 1, pp. 361–367, 1997.
- [22] V. Korenivski and R. B. van Dover, “Design of high frequency inductors based on magnetic films”, *IEEE Transactions on Magnetics*, vol. 34, pp. 1375–1377, 1998.
- [23] J. Y. Park and M. G. Allen, “High current integrated microinductors and microtransformers using low temperature fabrication processes”, in *Proceedings. 1996 International Symposium on Microelectronics (SPIE Vol.2920)*, pp. 120–5, 1996.
- [24] Y. Sasaki, S. Morita, T. Hatanai, A. Makino, T. Sato, and K. Yamasawa, “High frequency soft magnetic properties of nanocrystalline Fe-(Co)-Hf-O films with high electrical resistivity and their application to micro DC-DC converter”, *NanoStructured Materials*, vol. 8, pp. 1025–1032, 1997.
- [25] C. R. Sullivan and S. R. Sanders, “Design of microfabricated transformers and inductors for high-frequency power conversion”, *IEEE Trans. on Power Electronics*, vol. 11, pp. 228–238, 1996.
- [26] Ming Xy, Tirfon M. Liakopoulos, Chong H. Ahn, Suk Hee Han, and Hi Jung Kim, “A microfabricated transformer for high-frequency power or signal conversion”, *IEEE Transactions on Magnetics*, vol. 34, pp. 1369–1371, 1998.
- [27] S. Ohnuma, H. Fujimori, S. Mitani, and T. Masumoto, “High-frequency magnetic properties in metal-nonmetal granular films”, *Journal of Applied Physics*, vol. 79, pp. 5130–5135, 1996.
- [28] H. Fujimori, “Structure and 100mhz soft magnetic properties in multilayers and granular thin films”, *Scripta Metallurgica et Materialia*, vol. 33, pp. 1625–1635, 1995.
- [29] Y. Hayakawa and A. Makino, “Soft magnetic properties of Fe-M-O (M=Hf, Zr, Y, Ce) films with high electrical resistivity”, *NanoStructured Materials*, vol. 6, pp. 989–992, 1995.
- [30] Y. Hayakawa, A. Makino, H. Fujimori, and A. Inoue, “High resistive nanocrystalline Fe-M-O (M=Hf, Zr, rare-earth metals) soft magnetic films for high-frequency applications (invited)”, *J. Appl. Phys.*, vol. 81, pp. 3747–3763, 1997.
- [31] R. E. Jones, Jr., J. Williams, L. Spector, E.J. Lin, S. Wang, S. Pichai, and B. M. Clemens, “Magnetic properties of NiFe sputtered on sloping surfaces.”, *IEEE Trans. on Magnetics*, vol. 31, pp. 3817–19, 1995.
- [32] Pei-Hui Zheng, J. A. Bain, and M. H. Kryder, “The effect of surface topography on the soft magnetic properties of FeAlN films.”, *IEEE Trans. on Magnetics*, vol. 31, pp. 2700–2702, 1995.
- [33] Y. Nakagawa, Y. Ohshita, and S. Narishige, “Composition distribution and magnetic characteristics of sputtered permalloy films with substrate angle”, *Journal of Vacuum Science and Technology*, vol. A 7, pp. 1397–1401, 1989.
- [34] T. Inoue, K. Mishijima, S. Yatabe, and T. Mizoguchi, “The effects of magnetic film structure on the inductance of a planar inductor”, *IEEE Transactions on Magnetics*, vol. 34, pp. 1372–1373, 1998.
- [35] C. R. Sullivan and S. R. Sanders, “Microfabrication process for high-frequency power-conversion transformers”, in *26th Annual Power Electronics Specialists Conf.*, pp. 658–64, June 1995.
- [36] C. R. Sullivan and S. R. Sanders, “Microfabrication of transformers and inductors for high frequency power conversion”, in *24th Annual Power Electronics Specialists Conf.*, pp. 33–40, June 1993.
- [37] S. Ohnuma, N. Kobayashi, T. Masumoto, S. Mitani, and H. Fujimori, “Magnetostriiction and soft magnetic properties of highly electrical-resistive (Co<sub>1-x</sub>Fe<sub>x</sub>)-Al-O films”, in *The 43rd Annual Conference on Magnetism and Magnetic Materials—Abstracts*, p. 50, Nov. 1998.
- [38] S. Ramo, J. Whinnery, and T. Van Duzer, *Fields and Waves in Communication Electronics 3rd Ed.*, John Wiley and Sons, INC., 1994.